HUNGARIAN JOURNAL OF
INDUSTRY AND CHEMISTRY
Vol. 53(1) pp. 27–37 (2025)
hjic.mk.uni-pannon.hu
DOI: 10.33927/hjic-2025-04

HUNGARIAN JOURNAL OF INDUSTRY AND CHEMISTRY
HJIC

COMPARATIVE ANALYSIS OF MACHINE MODEL-BASED SENSORLESS DTC OF TWO PARALLEL CONNECTED FIVE-PHASE INDUCTION MACHINES

KHALED MOHAMMED SAID BENZAOUI[1]*, SIFELISLAM GUEDIDA[2], AHMED ZOUHIR KOUACHE[1] AND ELAKHDAR BENYOUSSEF[1]

1 Laboratoire LAGE, Faculté des Sciences Appliquées, Université Kasdi Merbah Ouargla, Ouargla, 30000, ALGERIA
2 École Militaire Polytechnique, UER ELT, Algiers, 16111, ALGERIA

In high-performance vector control methods, especially for critical applications, accurate and precise information about the state variables of a machine (speed, flux and torque) is necessary. Nevertheless, environmental conditions such as temperature, vibrations and EMI affect the performance of sensors. Sensorless control is a potential solution to address the aforementioned drawbacks as well as further enhance the reliability and performance of the system, in addition to reducing the cost and the size of the drive. Therefore, this work provides a comparative study of three different sensorless approaches of measuring the stator flux and speed estimation for the direct torque control (DTC) of two five-phase induction machines (FPIM) connected in parallel to a single two-level inverter based on a model reference adaptive system (MRAS), sliding mode observer (SMO) and high-gain observer (HGO). The independent control of such a drive is possible due to the additional degrees of freedom (DOF) provided by the five-phase system and the suitable rearrangement of phases. The open-loop estimator used in conventional DTC for estimating flux leads to drift and initial value problems as a result of using the pure integration method. Finally, an analytical study of the robustness, stability and effectiveness of the discussed sensorless control schemes is verified in terms of reference command tracking, low-speed operation and disturbance rejection.

Keywords: sensorless direct torque control (DTC), sliding mode observer (SMO), model reference adaptive system (MRAS), high-gain observer (HGO), two parallel-connected FPIMs

1. Introduction

Highly reliable and high-power critical applications such as in ship propulsion, electric vehicles and electric aircraft are the most suited applications for five-phase induction machines (FPIM) and permanent magnet synchronous machines (PMSM) [1]-[3]. This is due to several advantages that they boast, for instance, reduced current rating per phase, less flux and torque ripples as well as increased torque density on top of their fault-tolerant operation and additional degrees of freedom (DOF) compared to three-phase induction machines [4],[5]. These DOFs can be employed to achieve drive in two independent parallel-connected machines fed by a single inverter where the two machines operate independently under different conditions such as speed and load torque [6].

The direct torque control (DTC) of the FPIM is simple compared to field-oriented control and less sensitivity to the parameters of the machine with the decoupled control of the flux and torque of the FPIM enabling high dynamic performance [7],[8].

The working principle of DTC is based on choosing the optimal voltage vector (VV) to be applied in each sampling period in order to obtain the desired level of performance regarding the stator flux and electromagnetic torque requirements [9].

High-quality speed and flux sensors, such as incremental encoders and the Hall effect, are a crucial part of vector control for drive systems like in automotive applications. Nevertheless, environmental conditions, costs and the sheer size of the system restrict their application in drive systems. Moreover, flux sensors require the machine to be redesigned. As a result, developing a speed and flux sensorless approach is greatly sought. Since mechanical sensors are heavy and susceptible to malfunction under demanding conditions, resulting in the degradation of the inherited robustness of the FPIM, sensorless technologies can improve the reliability and robustness of the drive system [10].

Received: 19 Sept 2024; Revised: 6 Nov 2024;
Accepted: 11 Nov 2024
*Correspondence: benzaoui.khaled@univ-ouargla.dz

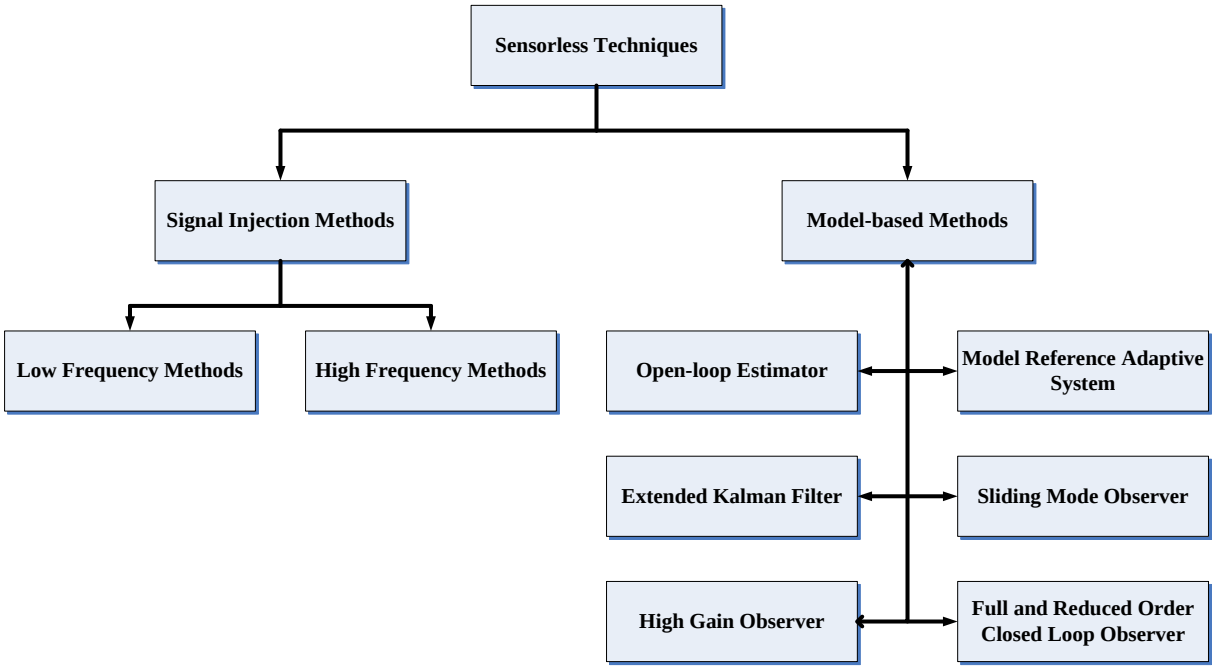

Figure 1: Classification of sensorless control techniques

As mentioned above, sensorless drive systems have attracted considerable attention over the last few years since implementing sensors increases hardware complexity and reduces noise immunity. Therefore, numerous methods for estimating the rotor speed and stator flux have been introduced to date classified as signal injections and machine model-based methods [11], as illustrated in *Figure 1*.

The first method is the signal injection technique, which can be further classified into high-frequency and low-frequency methods. Meanwhile, good performance at low speeds and when stationary as well as reduced parameter sensitivity are achieved. Regardless, these methods require additional hardware, resulting in severe skin effects due to the injected signal and noticeable electromagnetic torque ripples. Furthermore, the machines need to be redesigned. The state-of-the-art nature of signal injection methods has been reported [11],[12].

The second method is a machine model-based (MM) technique, where the machine model and measured parameters (stator voltages and currents) are used to estimate state variables following a specific structure and direct physical phenomena interpretation. Such methods have gained much attention in the literature [10],[11].

Estimating the rotor speed using the model reference adaptive system (MRAS) is based on the error between the output of two models, that is, the reference and adjustable model, which is fed into an adaptive model to estimate the rotor speed. This approach is known for its accuracy, simplicity and ease of implementation [13]. In [14], a sliding mode observer (SMO) for the sensorless application of an induction machine was proposed. The SMO is comprised of a sliding surface and control law, ensuring the state variables are accurately estimated with reduced sensitivity to parameter variations and a faster dynamic response. The high-gain observer (HGO) can estimate state variables of the system based on the canonical form and reject model uncertainties. Furthermore, its simple structure and fast dynamic response have drawn interest concerning the sensorless control application of induction machines [15].

Therefore, this manuscript provides a comparative analysis of the three MM-based sensorless solutions, namely MRAS, SMO and HGO. Considering the merits and disadvantages of each technique, the structure of this paper is as follows: Section 2 describes the modeling of a dual parallel-connected FPIM drive. Section 3 deals with the DTC of the drive of the two machines. The MM-based sensorless schemes are described in detail in Section 4. In Section 5, the simulation results are interpreted. Finally, in the last section, conclusions are drawn.

2. Modelling drive

The circuit diagram of the two FPIMs connected in parallel powered from a single two-level inverter is shown in *Figure 2*.

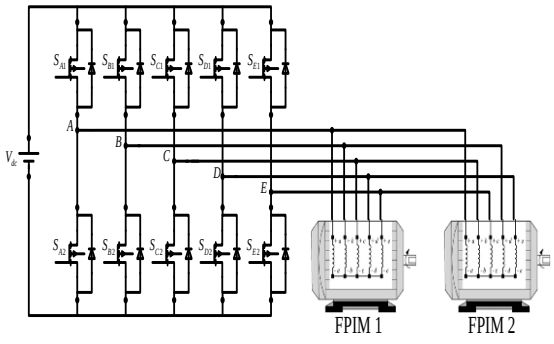

Figure 2: Schematic diagram of two FPIM drives connected in parallel

The relationship between the inverter and the voltage of both machines is discussed as follows:

$$\begin{bmatrix} v_A^{inv} \\ v_B^{inv} \\ v_C^{inv} \\ v_D^{inv} \\ v_E^{inv} \end{bmatrix} = \begin{bmatrix} v_{SA1} = v_{SA2} \\ v_{SB1} = v_{SC2} \\ v_{SC1} = v_{SE2} \\ v_{SD1} = v_{SB2} \\ v_{SE1} = v_{SD2} \end{bmatrix} \quad (1).$$

The Clarke's transformation matrix [C] describes the five-phase system in two orthogonal planes, $\alpha\beta_1$ and $\alpha\beta_2$, as well as in terms of a zero sequence component as follows [16]:

$$[C] = \frac{2}{5}\begin{bmatrix} 1 & \cos(2\pi/5) & \cos(4\pi/5) & \cos(6\pi/5) & \cos(8\pi/5) \\ 0 & \sin(2\pi/5) & \sin(4\pi/5) & \sin(6\pi/5) & \sin(8\pi/5) \\ 1 & \cos(6\pi/5) & \cos(2\pi/5) & \cos(8\pi/5) & \cos(4\pi/5) \\ 0 & \sin(6\pi/5) & \sin(2\pi/5) & \sin(8\pi/5) & \sin(4\pi/5) \\ \frac{1}{2} & \frac{1}{2} & \frac{1}{2} & \frac{1}{2} & \frac{1}{2} \end{bmatrix} \quad (2).$$

The considered machines consist of five distributed star-connected windings spatially shifted by 72 electrical degrees. The two machines model in the stationary reference frame, described assuming the same simplifying assumption applied in three-phase machines, is given below [17]:

$$\begin{cases} V_{sj\alpha\beta j} = R_{sj} i_{sj\alpha\beta j} + \dfrac{d\phi_{sj\alpha\beta j}}{dt} \\ 0 = R_{rj} i_{rj\alpha\beta j} + \dfrac{d\phi_{rj\alpha\beta j}}{dt} \\ \phi_{s\alpha\beta j} = L_{sj} i_{s\alpha\beta j} + L_{mj} i_{rj\alpha\beta j} \\ \phi_{sj\alpha\beta j} = L_{sj} i_{sj\alpha\beta j} \\ \phi_{rj\alpha\beta j} = L_{rj} i_{rj\alpha\beta j} + L_{mj} i_{sj\alpha\beta j} \\ \phi_{rj\alpha\beta j} = L_{rj} i_{rj\alpha\beta j} \end{cases} \quad (3).$$

The electromagnetic torque is given as:

$$T_{emj} = \frac{5 p_j L_{mj}}{\sigma_j L_{sj} L_{rj}} \phi_{sj} \phi_{rj} \sin\delta_j \quad (4),$$

where: j = 1 or 2, $V_{sj\alpha\beta j}$ stator voltages, $i_{sj\alpha\beta j}$ stator currents, $\phi_{s\alpha\beta j}$ stator flux linkages, $i_{rj\alpha\beta j}$ rotor currents, $\phi_{r\alpha\beta j}$ rotor flux linkages, R_s stator resistance, L_s stator leakage inductance, L_m mutual inductance, R_r rotor resistance, L_r rotor leakage inductance, T_{em} electromagnetic torque and p pair poles.

3. Direct torque control

The DTC scheme is based on the direct application of the optimal VV to the drive, which is further explained by *Equation 4*. Over a sampling period, the stator flux is assumed to be constant due to the high time constant of the rotor circuit compared to the stator circuit [18]. From *Equation 3*, the stator flux is described as follows in the plane $\alpha\beta_j$:

$$\hat{\phi}_{sj\alpha\beta j} = \int (v_{sj\alpha\beta j} - R_{sj} i_{sj\alpha\beta j}) dt \quad (5).$$

By neglecting the drop in the resistance voltage, *Equation 5* can be written as:

$$\hat{\phi}_{sj\alpha\beta j} = \int v_{sj\alpha\beta j} dt \quad (6).$$

Therefore, by applying the optimal VV, the stator flux and electromagnetic torque angle δ are controlled (*Equation 4*) [18]. The implemented DTC for the proposed drive is shown in *Figure 3*.

Two-level and seven-level HCs are utilized to compare the error between the reference and estimated values of both the flux and torque of the machines, thereby determining the required response, namely to increase or decrease the flux and torque.

The obtained output of the HCs and the flux position are exploited to develop look-up table (*Table 1*) in order to select the optimal VV. The VVs of the two-level inverter are illustrated in *Figure 4*.

Control of the two-machine drive requires two independent DTC controllers. Therefore, one controller is developed in the $\alpha\beta_1$ plane and the other in the $\alpha\beta_2$ plane taking into consideration the phase transposition given in *Equation 1* and *Figure 2,* resulting in the current components generating torque/flux for one machine but not for the other and vice versa [19].

For further explanation if the stator flux vector of the first FPIM is in Sector II and the stator flux needs to be increased ($\varepsilon_{\phi sj}$ =1) and decreasing the electromagnetic torque (ε_{Temj} =3). Therefore, from *Figure 4a*, the selected VV is VM4 with a switching sequence of 11110. Furthermore, if the stator flux of the second FPIM is within Sector VI and the stator flux must be decreased while increasing the electromagnetic torque ($\varepsilon_{\phi sj}$ =0, ε_{Temj} =3), the chosen VV is VL5 with a switching sequence of 01110 as shown in *Figure 4b*.

Table 1: The look-up table

ε_{Temj}	$\varepsilon_{\phi sj}$	
	-1	1
3	VL(i+4)	VL(i+1)
2	VM(i+4)	VM(i+1)
1	VS(i+4)	VS(i+1)
0	V0	V0
-1	VS(i+6)	VS(i+9)
-2	VM(i+6)	VM(i+9)
-3	VL(i+6)	VL(i+9)

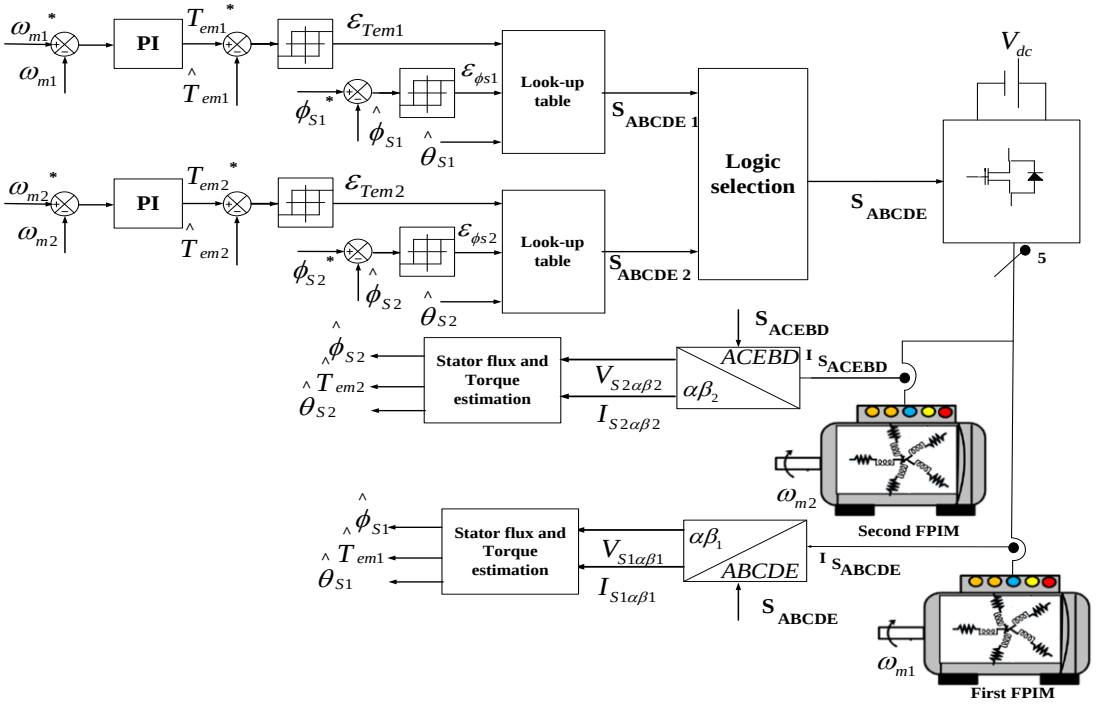

Figure 3: DTC of two FPIMs connected in parallel

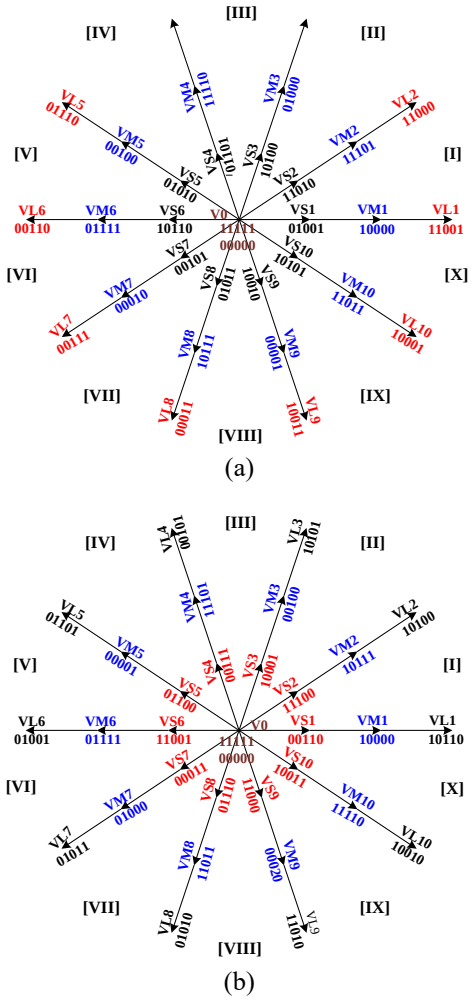

Figure 4: Mapping VVs: (a) in the $\alpha\beta_1$ plane, (b) in the $\alpha\beta_2$ plane

The logic selection block alternates between the two selected VVs throughout the whole sampling period. For example, when VM4 is applied to the inverter over the first sampling period and VL5 over the second.

4. Machine model (MM)-based sensorless methods

The basic common schematic structure of the MM-based sensorless methods which consist of the stator flux and/or rotor speed observer are depicted in *Figure 5*.

This paper analyzes the principles of three MM-based stator flux and rotor speed observers.

4.1. Model reference adaptive system (MRAS)

The MRAS discussed herein was proposed in [20]. The main objective of this observer is to estimate the rotor's mechanical speed based on the measured stator voltages and currents. The MRAS constitutes three models as follows [21]:

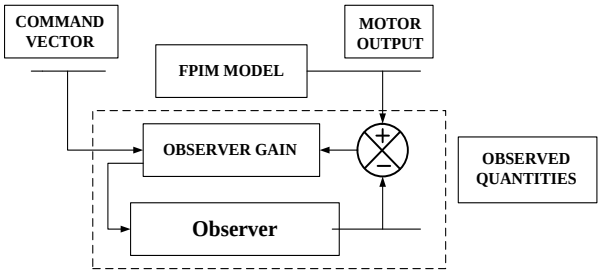

Figure 5: General presentation of the observers

The reference model

The voltage model of the machine is utilized given the independent nature of the mechanical speed of the rotor as follows:

$$\frac{d}{dt}\left[\phi_{rj}\right]_{\alpha\beta j}=\frac{L_{rj}}{L_{mj}}\left(\left[V_{sj}\right]_{\alpha\beta}-R_{sj}\left[I_{sj}\right]_{\alpha\beta j}-\sigma_j L_{sj}\left[I_{sj}\right]_{\alpha\beta j}\right) \quad (7).$$

The adaptive model

The stator current model of the FPIM is implemented, where the estimated mechanical speed of the rotor is integrated into the model to adjust the rotor flux.

$$\frac{d}{dt}\begin{bmatrix}\hat{\phi}_{rj}\end{bmatrix}_{\alpha\beta j}=\frac{L_{mj}}{T_{rj}}\begin{bmatrix}I_{sj\alpha j}\\ I_{sj\beta j}\end{bmatrix}-\frac{1}{T_{rj}}\begin{bmatrix}\hat{\phi}_{rj\alpha j}\\ \hat{\phi}_{rj\beta j}\end{bmatrix}+\omega_r\begin{bmatrix}-\hat{\phi}_{rj\alpha j}\\ \hat{\phi}_{rj\beta j}\end{bmatrix} \quad (8)$$

The adaptation mechanism

The error between the estimated values of the rotor flux obtained by the two models is entered into the adaptation mechanism to estimate the mechanical speed of the rotor as described in the following equation:

$$\begin{cases}\varepsilon_{estj}=\phi_{rj\beta j}\hat{\phi}_{rj\alpha j}-\phi_{rj\alpha j}\hat{\phi}_{rj\beta j}\\ \hat{\omega}_{rj}=K_{pj}\varepsilon_{estj}+K_{ij}\int\varepsilon_{estj}dt\end{cases} \quad (9).$$

The stator flux and electromagnetic torque can be calculated as follows:

$$\begin{cases}\hat{\phi}_{sj\alpha j}=\frac{L_{mj}}{L_{rj}}\hat{\phi}_{rj\alpha}+\frac{L_{sj}L_{rj}-L_{mj}^2}{L_{rj}}i_{sj\alpha j}\\ \hat{\phi}_{sj\beta j}=\frac{L_{mj}}{L_{rj}}\hat{\phi}_{rj\beta}+\frac{L_{sj}L_{rj}-L_{mj}^2}{L_{rj}}i_{sj\beta j}\\ \hat{\phi}_{sj}=\sqrt{\hat{\phi}_{sj\alpha j}^{\ 2}+\hat{\phi}_{sj\beta j}^{\ 2}}\\ \theta_{sj}=\tan^{-1}\left(\frac{\hat{\phi}_{sj\beta j}}{\hat{\phi}_{sj\alpha j}}\right)\\ \hat{T}_{emj}=\frac{5p_j}{2}\left(\hat{\phi}_{sj\alpha j}\,i_{sj\beta j}-\hat{\phi}_{sj\beta j}\,i_{sj\alpha j}\right)\end{cases} \quad (10).$$

The schematic diagram of the MRAS is illustrated in *Figure 6*.

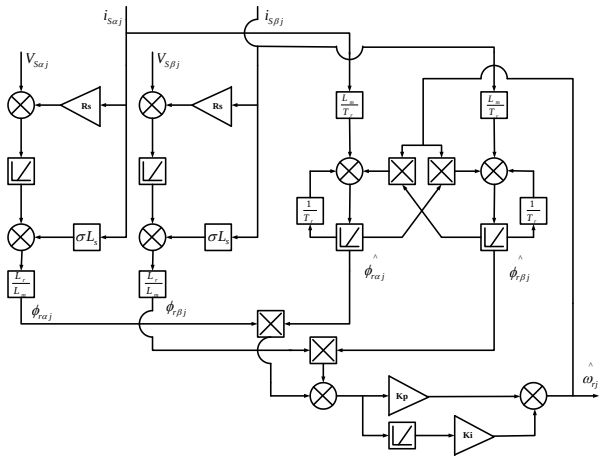

Figure 6: Schematic diagram of the MRAS

4.2. Sliding mode observer

In this control method, the sliding mode control is used to construct the stator flux and speed observer to reconstruct the FPIM variables. *Figure 7* shows the block diagram of the SMO.

The observer design is based on two aspects, namely the sliding surface and the control law, which control the estimation process. With reference to the FPIM model in the $\alpha\beta_j$ plane, the observer is expressed as follows [22]:

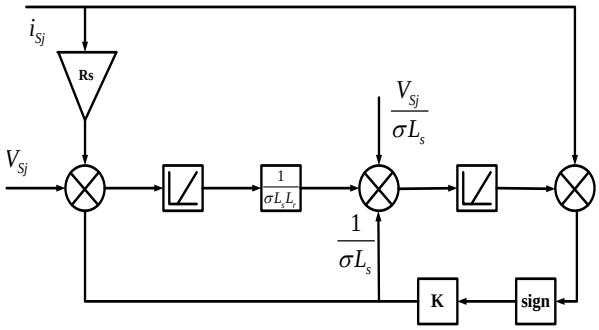

Figure 7: Schematic diagram of the SMO

$$\begin{cases}\frac{d\hat{i}_{s\alpha j}}{dt}=a_1\hat{i}_{s\alpha j}+a_6\hat{i}_{s\beta j}+a_2\hat{\phi}_{s\alpha j}+a_3\hat{\phi}_{s\beta j}+b_1V_{s\alpha j}+A_{i1}I_{s1}+A_{i2}I_{s2}\\ \frac{d\hat{i}_{s\beta j}}{dt}=-a_6\hat{i}_{s\alpha j}+a_1\hat{i}_{s\beta j}+a_3\hat{\phi}_{s\alpha j}+a_2\hat{\phi}_{s\beta j}+b_1V_{s\beta j}+A_{i3}I_{s1}+A_{i4}I_{s2}\\ \frac{d\hat{\varphi}_{s\alpha j}}{dt}=a_4\hat{i}_{s\alpha j}+V_{s\alpha j}+A_{\phi 1}I_{s1}+A_{\phi 2}I_{s2}\\ \frac{d\hat{\phi}_{s\beta j}}{dt}=a_4\hat{i}_{s\beta j}+V_{s\beta j}+A_{\phi 3}I_{s1}+A_{\phi 4}I_{s2}\end{cases} \quad (11),$$

where $\hat{i}_{s\alpha j},\hat{i}_{s\beta j}$ denote the estimated stator currents, $\hat{\varphi}_{s\alpha j},\hat{\varphi}_{s\beta j}$ represent the estimated stator flux components, ω_r stands for the estimated rotor speed, $A_{ix}\,(x=1,2,3,4)$ refer to the stator current gains and $A_{\varphi x}\,(x=1,2,3,4)$ are the stator flux gains.

The sliding surface is defined as:

$$I_s=\begin{bmatrix}I_{s1}\\ I_{s2}\end{bmatrix}=\begin{bmatrix}sign(S1)\\ sign(S2)\end{bmatrix} \quad (12),$$

where: $\begin{cases}S1=i_{s\alpha j}-\hat{i}_{s\alpha j}\\ S2=i_{s\beta j}-\hat{i}_{s\beta j}\end{cases}$ (13).

The current and flux gains can be selected as follows:

$$\begin{bmatrix} A_{11} & A_{12} \\ A_{11} & A_{12} \end{bmatrix} = D \begin{bmatrix} \delta_1 & 0 \\ 0 & \delta_2 \end{bmatrix} \quad (14),$$

where $D = \begin{bmatrix} \frac{R_r}{\sigma L_s L_r} & \frac{\omega_r}{\sigma L_s} \\ -\frac{\omega_r}{\sigma L_s} & \frac{R_r}{\sigma L_s L_r} \end{bmatrix}$ (15)

and $\begin{bmatrix} A_{\phi 1} & A_{\phi 2} \\ A_{\phi 1} & A_{\phi 2} \end{bmatrix} = \begin{bmatrix} \left(q_1 - \frac{R_{rj}}{L_{rj}}\right)\delta_1 & \frac{\hat{\omega}_{rj}}{\sigma_j L_{sj}} \\ \frac{-\hat{\omega}_{rj}}{\sigma_j L_{sj}} & \left(q_1 - \frac{R_{rj}}{L_{rj}}\right)\delta_2 \end{bmatrix}$ (16),

where δ_1, δ_2, q_1 and q_2 are positive constants.

The stability of the observer is related to its convergence onto the sliding surface [22]. A Lyapunov function is proposed to solve this problem as follows:

$$V = \frac{1}{2} S^T S \quad (17).$$

Since the stability of the observer is related to the estimated stator flux and their convergence onto the sliding surface, the observation error should be equal to zero. For this to be so, the derivative of the Lyapunov function must be strictly negative.

$$\dot{V} = \frac{1}{2} S^T \dot{S} < 0 \quad (18)$$

Therefore, the stability of the observer is ensured if the inequality below is verified:

$$\begin{cases} \delta_1 \geq \left|\varepsilon_{\phi\alpha}\right| \\ \delta_2 \geq \left|\varepsilon_{\phi\beta}\right| \end{cases} \quad (19).$$

The stator flux vector and position, in addition to the rotor speed and electromagnetic torque, are computed as follows:

$$\begin{cases} \hat{\phi}_{sj} = \sqrt{\hat{\phi}_{sj\alpha j}^{\,2} + \hat{\phi}_{sj\beta j}^{\,2}} \\ \theta_{sj} = \tan^{-1}\left(\hat{\phi}_{sj\beta j} \,/\, \hat{\phi}_{sj\alpha j}\right) \\ \frac{d\hat{\omega}_{mj}}{dt} = 1/J_j\left(p_j(\hat{\phi}_{sj\alpha j} i_{sj\beta j} - \hat{\phi}_{sj\beta j} i_{sj\alpha j}) - \hat{T}_{Lj} - f_j \hat{\omega}_{mj}\right) \\ \hat{T}_{emj} = \frac{5p_j}{2}(\hat{\phi}_{sj\alpha j} i_{sj\beta j} - \hat{\phi}_{sj\beta j} i_{sj\alpha j}) \end{cases} \quad (20).$$

4.3. High-gain observer (HGO)

The HGO technique has attracted much attention for its simple design and ease of tuning. The HGO is designed to directly reconstruct the stator variables of the machine from the measured quantities (stator voltages and currents) [23]. The block diagram of the HGO is illustrated in *Figure 8*.

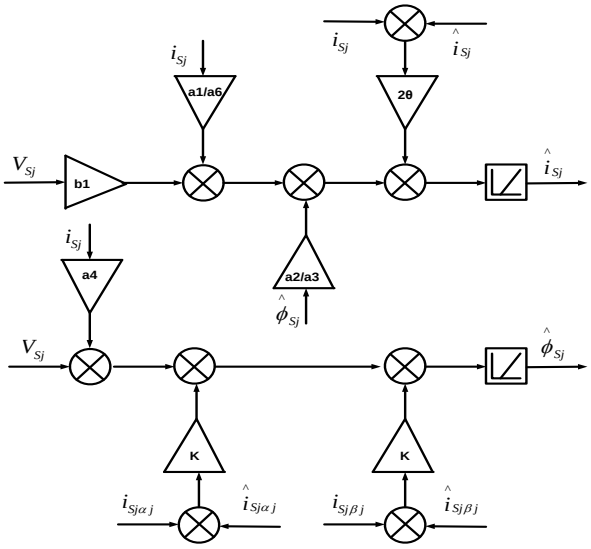

Figure 8: Schematic diagram of the HGO

The expression of the observer, based on the FPIM model, can be given as:

$$\begin{cases} \dot{\hat{x}} = A\hat{x} + Bu + \nu(e_m) \\ \nu(e_m) = \theta \wedge^{-1}(\hat{x}) V_\theta^{-1} S^{-1} C^T C e_m \end{cases} \quad (21),$$

$$\begin{cases} x = \begin{bmatrix} i_{s\alpha j} & i_{s\beta j} & \varphi_{s\alpha j} & \varphi_{s\beta j} \end{bmatrix}^T \\ e_m = \begin{bmatrix} i_{s\alpha j} - \hat{i}_{s\alpha j} & i_{s\beta j} - \hat{i}_{s\beta j} & 0 & 0 \end{bmatrix}^T \end{cases} \quad (22),$$

where x denotes the state variables and e_m the stator current error.

$$\begin{cases} V_{\theta 1} = diag(I_2, \frac{1}{\theta} I_2) \ \ with \ \theta > 0 \ \ (V_{\theta 1})^1 = diag(I_2, \theta I_2) \\ \wedge = diag(I_2, kF(\omega)) \ \ with \ \ \wedge^{-1} = diag(I_2, \frac{1}{k} F^{-1}(\omega)) \end{cases} \quad (23)$$

with $k = \frac{1}{\sigma L_s}$, $kF(\omega) = \begin{bmatrix} \frac{R_r}{\sigma L_s L_r} & \frac{\omega}{\sigma L_s} \\ -\frac{\omega}{\sigma L_s} & \frac{R_r}{\sigma L_s L_r} \end{bmatrix}$ (24),

where S represents the peculiar solution of the Lyapunov function.

$$\begin{cases} S + A^T S + SA = C^T C \\ S^{-1} C = \begin{bmatrix} C_2^1 I_2 & C_2^2 I_2 \end{bmatrix} = \begin{bmatrix} 2I_2 & I_2 \end{bmatrix} \end{cases} \quad (25)$$

Replacing $\nu(e_m)$ in *Equation 21* yields:

$$\begin{cases} \dfrac{d\hat{i}_{s\alpha j}}{dt} = a_1 i_{s\alpha j} + a_6 i_{s\beta j} + a_2 \varphi_{s\alpha j} + a_3 \varphi_{s\beta j} + b_1 V_{s\alpha j} + 2\theta(i_{s\alpha j} - \hat{i}_{s\alpha j}) \\ \dfrac{d\hat{i}_{s\beta j}}{dt} = -a_6 i_{s\alpha j} + a_1 i_{s\beta j} + a_3 \varphi_{s\alpha j} + a_2 \varphi_{s\beta j} + b_1 V_{s\beta j} + 2\theta(i_{s\beta j} - \hat{i}_{s\beta j}) \\ \dfrac{d\hat{\varphi}_{s\alpha j}}{dt} = a_4 i_{s\alpha j} + V_{s\alpha j} + \theta^2 \dfrac{a_2}{a_2^{\,2} + a_3^{\,2}}(i_{s\alpha j} - \hat{i}_{s\alpha j}) - \theta^2 \dfrac{a_3}{a_2^{\,2} + a_3^{\,2}}(i_{s\beta j} - \hat{i}_{s\beta j}) \\ \dfrac{d\hat{\varphi}_{s\beta j}}{dt} = a_4 i_{s\beta j} + V_{s\beta j} + \theta^2 \dfrac{a3}{a_2^{\,2} + a_3^{\,2}}(i_{s\alpha j} - \hat{i}_{s\alpha j}) - \theta^2 \dfrac{a_2}{a_2^{\,2} + a_3^{\,2}}(i_{s\beta j} - \hat{i}_{s\beta j}) \end{cases} \quad (26),$$

where $a_1 = -\left(\dfrac{R_s + R_r}{\sigma L_s}\right)$, $a_2 = \dfrac{R_r}{\sigma L_s L_r}$, $a_3 = \dfrac{\omega}{\sigma L_s}$, $a_4 = -R_s$, $a_6 = -\omega_r$, $b_1 = \dfrac{1}{\sigma L_s}$ and θ is the observer gain.

Estimation of the speed and torque are achieved based on the following formula:

$$\begin{cases} \dfrac{d\hat{\omega}_j}{dt} = 1/J(p_j(\hat{\phi}_{s\alpha j} i_{s\beta j} - \hat{\phi}_{s\beta j} i_{s\alpha j}) - T_L - f\hat{\omega}_j) \\ \hat{T}_{em} = p_j(\hat{\phi}_{s\alpha j} i_{s\beta j} - \hat{\phi}_{s\beta j} i_{s\alpha j}) \end{cases} \quad (27).$$

5. Simulation results

This section uses simulation tests to evaluate the performance of the three MM-based observers in their transient/steady state and at low speeds as well as by taking into consideration implementation complexity and computational burden. The parameters of the two machines are depicted in *Table 2*.

5.1. First test

The performance of the three MM-based sensorless methods is evaluated at different speeds, such as low and high, under their rated load torque. The test scenarios are summarized in *Tables 3 and 4*.

5.2. Second test

This test examines the robustness and disturbance rejection of the three MM-based sensorless methods when the load torque is suddenly changed. The test scenario is described in *Table 5*.

5.3. Discussion

The discussed MM-based sensorless methods to estimate accuracy using the FPIM over a wide range of reference speeds and by varying the load torque is evaluated (*Figures 9-18*).

In *Figures 9* and *14*, the rotor speed responses of the two machines are shown. When the drive is operated in its steady and transient states, the speed of the machines

Table 2: Parameters of the machine

1 Hp ; 200 V; 50 Hz; 1400 rpm	
R_s [Ω]	10
R_r [Ω]	6.3
L_s [Ω]	0.4642
L_r [Ω]	0.4612
L_m [H]	0.4212
J [$Kg.m^2$]	0.03
f [$\frac{Nm.s^{-1}}{rad}$]	0.0001
T_{em} [$N.m$]	8
p	2

Table 3: Test scenario of the first FPIM

$Time[s]$	$\omega_m[rad/s]$	$T_L[Nm]$
$0 \to 0.1$	$0 \to 20$	8
$0.1 \to 1$	20	
$1 \to 1.3$	$20 \to 60$	
$1.3 \to 2$	60	
$2 \to 2.2$	$60 \to 100$	
$2.2 \to 3$	100	
$3 \to 4$	$100 \to -100$	
$4 \to 4.5$	-100	

Table 4: Test scenario of the second FPIM

$Time[s]$	$\omega_m[rad/s]$	$T_L[Nm]$
$0 \to 0.5$	$0 \to -100$	8
$0.5 \to 2$	-100	
$2 \to 2.6$	$-100 \to 20$	
$2.6 \to 3.4$	20	
$3.4 \to 3.7$	$20 \to 60$	
$3.7 \to 4.2$	60	
$4.2 \to 4.4$	$60 \to 100$	
$4.4 \to 5$	100	

Table 5: Second test scenario

$Time[s]$	$\omega_m[rad/s]$	$T_{L1}[Nm]$	$T_{L2}[Nm]$
$0 \to 0.5$	$0 \to 100$	8	-2
$0.5 \to 1$			
$1 \to 2$	100	0	8
$2 \to 3$		-4	0

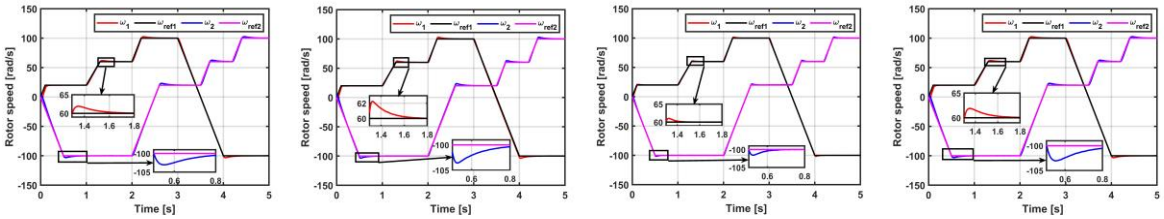

(a) (b) (c) (d)

Figure 9: Rotor speed response: (a) DTC, (b) MRAS, (c) SMO and (d) HGO

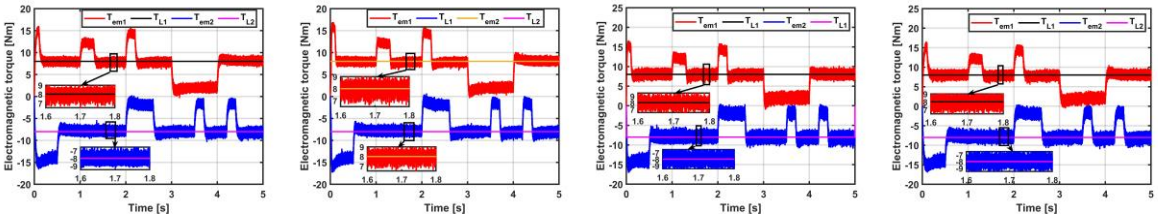

(a) (b) (c) (d)

Figure 10: Electromagnetic torque response: (a) DTC, (b) MRAS, (c) SMO and (d) HGO

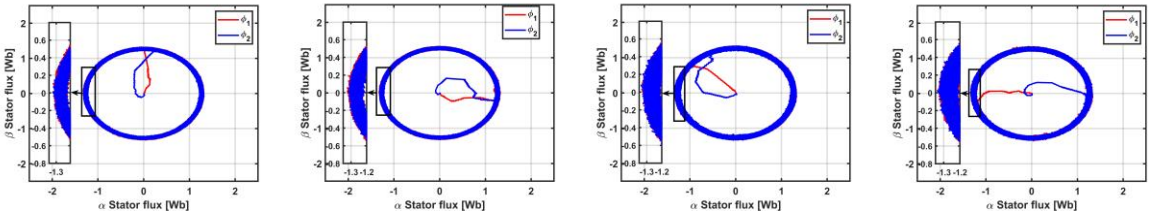

(a) (b) (c) (d)

Figure 11: Stator flux response: (a) DTC, (b) MRAS, (c) SMO and (d) HGO

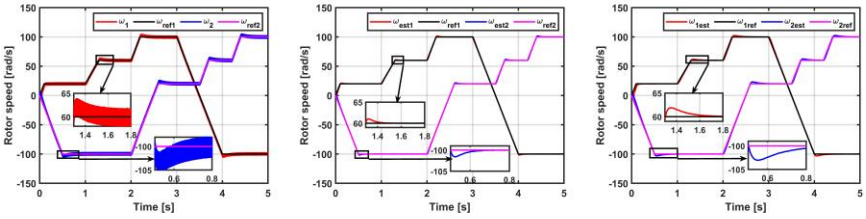

(a) (b) (c)

Figure 12: Estimated rotor speed: (a) MRAS, (b) SMO and (c) HGO

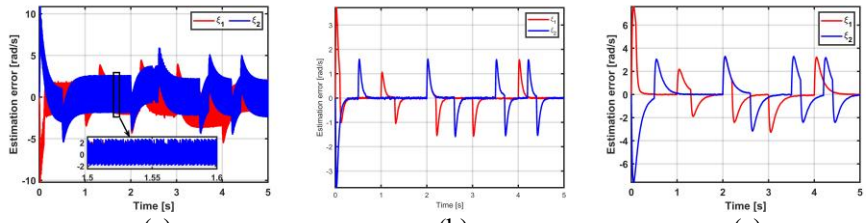

(a) (b) (c)

Figure 13: Estimation error: (a) MRAS, (b) SMO and (c) HGO

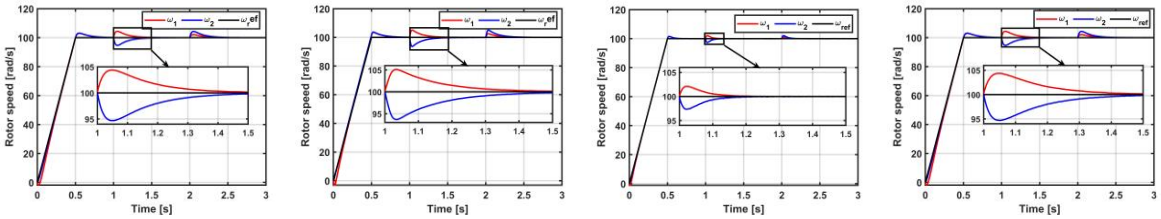

(a) (b) (c) (d)

Figure 14: Rotor speed response: (a) DTC, (b) MRAS, (c) SMO and (d) HGO

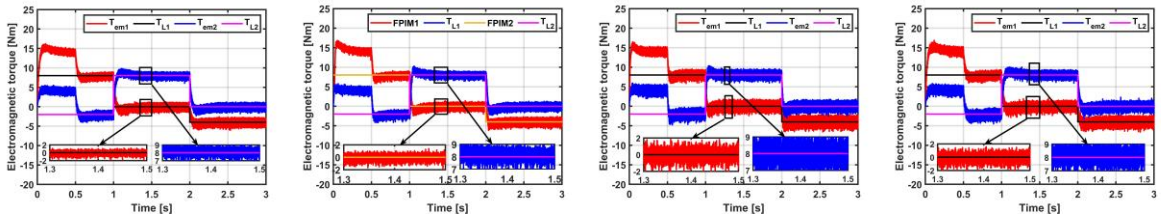

(a) (b) (c) (d)

Figure 15: Electromagnetic torque response: (a) DTC, (b) MRAS, (c) SMO and (d) HGO

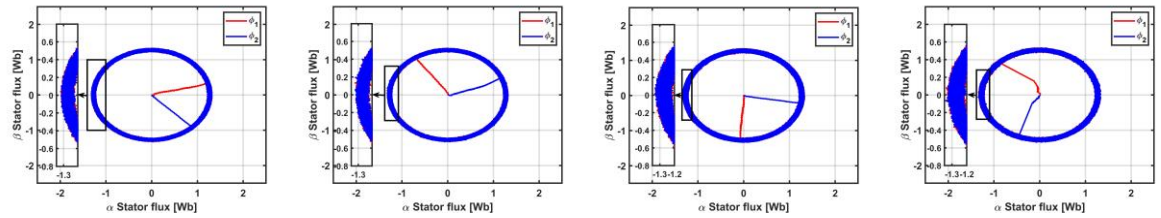

(a) (b) (c) (d)

Figure 16: Stator flux response: (a) DTC, (b) MRAS, (c) SMO and (d) HGO

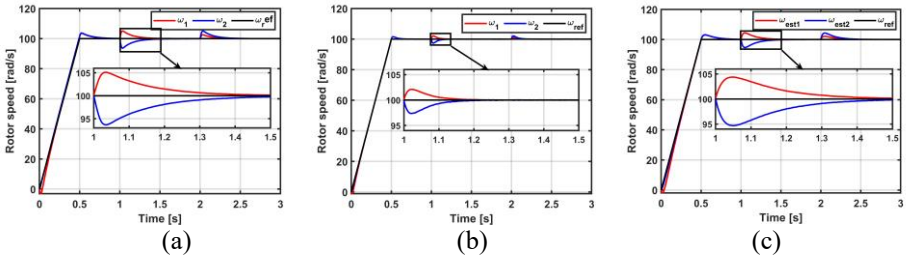

(a) (b) (c)

Figure 17: Estimated rotor speed: (a) MRAS, (b) SMO and (c) HGO

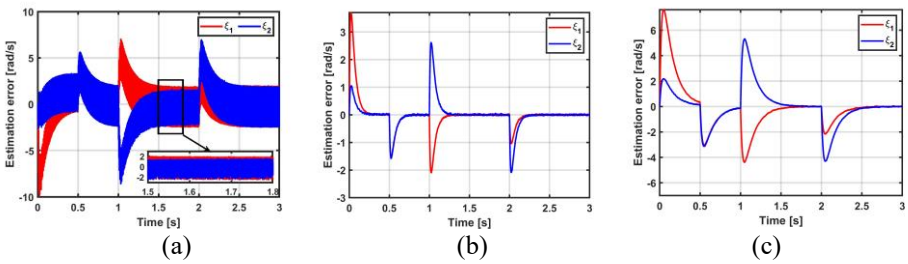

(a) (b) (c)

Figure 18: Estimation error: (a) MRAS, (b) SMO and (c) HGO

Table 6: Performance comparison of the MM sensorless techniques

Assessment parameters		DTC	DTC-MRAS	DTC-SMO	DTC-HGO
ω_m	Recovery time (s)	0.3	0.5	0.5	0.3
	Overshoot (rad/s)	2	5	2	5
	Undershoot (rad/s)	2	5	2	5
	Estimation error (rad/s)	-	±4	±3	±6
ϕ_s	Ripples (Wb)	0.1894	0.0988	0.1889	0.1452
T_{em}	Ripples (Nm)	3.6607	3.4262	3.3775	3.7638

Table 7: Comparative analysis of the MM sensorless methods

	MRAS	SMO	HGO
Steady-state error	Very good	Excellent	Very good
Dynamic behaviour	Good	Excellent	Good
Low-speed operation	Satisfactory	Very good	Satisfactory
Complexity	Very good	Satisfactory	Excellent
Computation time	Good	Very good	Very good

accurately follows reference commands regardless of the loading conditions of both machines with negligible over/undershoot.

The estimated rotor speeds for the three observers are illustrated in *Figures 12* and *17*, respectively. These results show that the three methods accurately track the reference speed applied to the drive using different estimation errors, namely 4 rad/s for MRAS, ±3 rad/s for SMO and ±6 rad/s for HGO as presented in *Figures 13* and *18*, respectively.

Given the electromagnetic torque response shown in *Figures 10* and *15*, it is quickly interpreted that in response to changes in speed and the load torque applied, the electromagnetic torque is precisely and quickly determined corresponding to the load torque in the steady state.

The stator flux response exhibiting a circular trajectory following the reference command as well as a good degree of decoupling between the stator flux and electromagnetic torque of the two FPIMs is depicted in *Figures 11* and *16*.

Therefore, neither the transient state nor sensorless operation affects the performance of the two-machine drive. The test results are summarized in *Table 6* where a slight reduction in the torque and flux ripples is due to the accurate estimation of the three observers as opposed to the open-loop estimator used in the conventional method.

An analytical comparison is given in *Table 7* between the discussed sensorless control schemes based on a set of performance criteria. When compared to the SMO, the structures of the HGO and MRAS observers are less complex, only requiring one or two parameters to be tuned. However, the SMO performs better during the steady and transient states at high and low speeds with negligible estimation errors.

6. Conclusions

An analytical study of three machine model-based sensorless schemes for a two-FPIM drive connected in parallel is presented where the sensorless operation of this two-machine drive is evaluated over a wide range of operations based on several criteria such as dynamic performance, low-speed operations as well as robustness to external disturbances such as variation in load torque, computational burden and implementation complexity. As illustrated in the simulation results, the three sensorless control schemes, namely the model reference adaptive system (MRAS), sliding mode observer (SMO) and high-gain observer (HGO), perform satisfactorily considering the reference speed and tracking of load torque when disturbances are ignored. However, among these schemes based on the merits and demerits discussed herein, the sliding mode observer (SMO) performs better in terms of its estimation error, dynamic behavior and computation time with only one drawback, that is, the necessity to tune multiple gains.

REFERENCES

[1] Levi, E.: Multiphase electric machines for variable-speed applications, *IEEE Trans. Ind. Electron.*, 2008, **55**(5), 1893–1909, DOI: 10.1109/tie.2008.918488

[2] Babangida, A.; Szemes, P.T.: Electric vehicle modelling and simulation of a light commercial vehicle using PMSM propulsion, *Hung. J. Ind. Chem.*, 2021, **49**(1), 37–46, DOI: 10.33927/hjic-2021-06

[3] Benzaoui, K.M.S.; Benyoussef, E.; Guedida, S.; Tabbache, B.; Kouache, A.Z.: Sensorless DTC based on artificial neural network for independent control of dual 5-phase induction machine fed by a three-level NPC inverter, *Adv. Electr. Electron. Eng.*, 2024, **22**(3), 281–296, DOI: 10.15598/aeee.v22i3.5738

[4] Kulandaivel, G.; Sundaram, E.; Gunasekaran, M.; Chenniappan, S.: Five-phase induction motor drive - A comprehensive review, *Front. Energy Res.*, 2023, **11**, 1178169, DOI: 10.3389/fenrg.2023.1178169

[5] Nesri, M.; Nounou, K.; Sifelislam, G.; Benkhoris, M.F.; Azeddine, H.: Hybrid flatness-based control of dual star induction machine drive system for more electrical aircraft, *Power Electron. Drives*, 2024, **9**(1), 50–62, DOI: 10.2478/pead-2024-0004

[6] Saadeh, O.; Dalbah, M.; Dalala, Z.: Control of two five-phase parallel connected single source motor drives under balanced and unbalanced conditions, *Proc. 9th IEEE Int. Symp. Power Electron. Distrib. Gener. Syst. PEDG (preprint)*, Charlotte, NC, USA, 2018, pp. 1–6, DOI: 10.1109/pedg.2018.8447807

[7] Khadar, S.; Abu-Rub, H.; Kouzou, A.: Sensorless field-oriented control for open-end winding five-phase induction motor with parameters estimation, *IEEE Open J. Ind. Electron. Soc.*, 2021, **2**, 266–279, DOI: 10.1109/ojies.2021.3072232

[8] Guedida, S.; Tabbache, B.; Nounou, K.; Benbouzid, M.: Direct torque control scheme for less harmonic currents and torque ripples for dual star induction motor, *Rev. Roum. Sci. Tech.-Él.*, 2023, **68**(4), 331–338, DOI: 10.59277/rrst-ee.2023.4.2

[9] Krishna, U.H.; Rajeevan, P.P.: A direct torque control scheme for five-phase induction motor drive with reduced current distortion, *Proc. 8th IEEE India Int. Conf. Power Electron. (IICPE)*, Jaipur, India, 2018, pp. 1–6, DOI: 10.1109/IICPE.2018.8709603

[10] Zaky, M.S.; Khater, M.; Yasin, H.; Shokralla, S.S.: Speed-sensorless control of induction motor drives, *Acta Electrothech.*, 2008, **49**(3), 251–268

[11] Alsofyani, I.M.; Idris, N.R.N.: A review on sensorless techniques for sustainable reliablity and efficient variable frequency drives of induction motors, *Renew. Sustain. Energy Rev.*, 2013, **24**, 111–121, DOI: 10.1016/j.rser.2013.03.051

[12] Xu, D.; Wang, B.; Zhang, G.; Wang, G., Yu, Y.: A review of sensorless control methods for AC motor drives, *CES Trans. Electr. Mach. Syst.*, 2018, **2**(1), 104–115, DOI: 10.23919/tems.2018.8326456

[13] El Merrassi, W.; Abounada, A.; Ramzi, M.: Advanced speed sensorless control strategy for induction machine based on neuro-MRAS observer, *Mater. Today Proc.*, 2021, **45**, 7615–7621, DOI: 10.1016/j.matpr.2021.03.081

[14] Ghanes, M.: Observation et commande de la machine asynchrone sans capteur mécanique (PhD thesis), 2005, Université de Nantes, Nantes, France, https://theses.hal.science/tel-00117094/

[15] Kadrine, A.; Tir, Z.; Malik, O.P.; Hamida, M.A.; Reatti, A.; Houari, A.: Adaptive non-linear high gain observer based sensorless speed estimation of an induction motor, *J. Franklin Inst.*, 2020, **357**(13), 8995–9024, DOI: 10.1016/j.jfranklin.2020.06.013

[16] Benzaoui, K.M.S.; Benyoussef, E.; Kouache, A.Z.: Three-level direct torque control based on common mode voltage reduction strategy fed two parallel connected five-phase induction machine, *Rev. Roum. Sci. Tech.-Él.*, 2024, **69**(2), 177–182, DOI: 10.59277/rrst-ee.2024.2.10

[17] Bermudez, M.; Gonzalez-Prieto, I.; Barrero, F.; Guzman, H.; Duran, M.J.; Kestelyn, X.: Open-phase fault-tolerant direct torque control technique for five-phase induction motor drives, *IEEE Trans. Ind. Electron.*, 2017, **64**(2), 902–911, DOI: 10.1109/tie.2016.2610941

[18] Tatte, Y.N.; Aware, M.V.: Torque ripple minimization in five-phase three-level inverter fed direct torque control induction motor drive, *Proc. 2015 17th Eur. Conf. Power Electron. Appl. (EPE'15 ECCE-Europe),* Geneva, Switzerland, 2015, pp. 1-6., DOI: 10.1109/EPE.2015.7309400

[19] Kamel, T.; Abdelkader, D.; Said, B.; Al-Hitmi, M.; Iqbal, A.: Sliding mode control based DTC of sensorless parallel-connected two five-phase PMSM drive system, *J. Electr. Eng. Technol.*, 2018, **13**(3), 1185–1201, DOI: 10.5370/JEET.2018.13.3.1185

[20] Sugimoto, H.; Tamai, S.: Secondary resistance identification of an induction-motor applied model reference adaptive system and its characteristics, *IEEE Trans. Ind. Electron.*, 1987, **IA-23**(2), 296–303, DOI: 10.1109/tia.1987.4504905

[21] Guedida, S.; Tabbache, B.; Benzaoui, K.M.S.; Nounou, K.; Nesri, M.: Novel speed sensorless DTC design for a five-phase induction motor with an intelligent fractional order controller based-MRAS estimator, *Power Electron. Drives*, 2024, **9**(1), 63–85, DOI: 10.2478/pead-2024-0005

[22] Benzaoui, K.M.S.; Benyoussef, E.; Kouache, A.Z.: Artificial neural network sensorless direct torque control of two parallel-connected five-phase induction machines, *Majlesi J. Electr. Eng.*, 2024, **18**(3), 1–14, DOI: 10.57647/j.mjee.2024.180348

[23] Jnayah, S.; Khedher, A.: Improvement of DTC performance of three level inverter fed IM drive with high gain flux observer, in: Digital technologies and applications – Proc. ICDTA 2022, Motahhir, S.; Bossoufi, B. (Eds), Lecture Notes in Networks and Systems (Springer, Cham), 2022, **454**, DOI: 10.1007/978-3-031-01942-5_78